

Modeling of InGaN/GaAs Photovoltaic Tandem with GaAs/AlAs Bragg Mirror Rear Surface Reflector

F. Bouzid*‡, N. Benaziez**

*Laboratory of Metallic and Semiconducting Materials, University of Biskra, P.B.145, Biskra, 07000, Algeria.

**Physics Department, Faculty of Sciences, University of Batna, Batna 05000, Algeria.

(faycal.bouzid@ymail.com, n.benaziez2@yahoo.com)

‡Corresponding Author; F. Bouzid, LMSM, University of Biskra, P.B.145, Biskra, 07000, Algeria,

Tel: +213 (0)33741087, Fax: +213 (0)33741087, faycal.bouzid@ymail.com

Received: 20.08.2014 Accepted: 07.09.2014

Abstract- In this work, a parametric study of a dual junction tandem based on $\text{In}_{0.53}\text{Ga}_{0.47}\text{N}$ on GaAs has been carried. In order to obtain reflection of unabsorbed photons from the bottom of the device, Bragg reflectors (BR) composed of GaAs/AlAs, with appropriate thicknesses, was placed in the rear surface of the GaAs sub-cell. With this intention, the current-voltage curves are calculated for different front recombination velocities and the influence of the bottom cell thickness on efficiency has been studied. The results of simulation show that the structure's efficiency can attain 29% under 1-sun AM1.5 illumination, for a front recombination velocity value of $1\text{e}^3\text{cm/s}$ and $10\mu\text{m}$ bottom cell thickness. This efficiency will decrease with increasing the operating temperature.

Keywords- Bragg Reflector; Carrier Lifetimes; Recombination Velocity; Efficiency; Temperature.

1. Introduction

Much research effort has been made on the improvement of multi-junction solar cells. The aim has been to raise the efficiency beyond the limit of single junction cells. This development has led to a great variety of multi-junction cells, which can be classified according to the materials used, the kind of combination of the junctions, mechanically stacked or monolithic and the number of terminals used to contact the device.

A tandem cell using Indium Gallium Nitride ($\text{In}_x\text{Ga}_{1-x}\text{N}$) cell on Gallium Arsenide (GaAs) cell is advantageous in two respects: $\text{In}_x\text{Ga}_{1-x}\text{N}$ alloy has a direct bandgap extends always since Indium Nitride (InN) bandgap which is 0.7eV in the medium infrared, to that of the Gallium Nitride (GaN) which is 3.42eV [1] in the near ultraviolet, makes the $\text{In}_x\text{Ga}_{1-x}\text{N}$ a potential radiation and temperature resistant alloy [2]. In the other hand, GaAs have been considered as a potential candidate for multi-junction cells for many purposes because

of its high efficiency. In addition, the GaAs bandgap of 1.42eV makes it highly resistant to radiation damage and relatively insensitive to heat.

One of the ways to diminish the solar power conversion losses, due to optical absorption, is to increase the optical path for weakly absorbed photons within the semiconductor. Bragg reflectors (BR), as rear surface reflectors, could provide the conditions for multi-passing of photons with energies close to the GaAs bandgap, through the photoactive region increasing the photocurrent. It is a structure produced from many layers of irregular materials with periodic disparity of refractive index. Every layer border leads to a partial reflection of an optical wave [3].

The ideal layer thicknesses in Bragg mirrors are $\lambda/4n$, where n is the refractive index of all of the materials and λ is the central wavelength of the reflected light [4].

An appropriate mirror with elevated reflectivity necessitates materials that have small absorption at the required operation wavelength, and a large index contrast is advantageous in order to keep the mirrors as thin as possible.

At least one material must have a large non-linear index of refraction to permit effective all-optical switching. GaAs and AlAs convene this condition [5]. Thus, it is useful to have a comprehensive analytical model of the $\text{In}_x\text{Ga}_{1-x}\text{N}$ on GaAs tandem solar cells behaviour.

In this paper, we have modelled the photovoltaic conversion efficiency of series-connected, two-junction, two-terminal $\text{In}_x\text{Ga}_{1-x}\text{N}$ on GaAs tandem solar cells in terms of their physical parameters, employing a simulation program developed for this reason, where the $\text{In}_x\text{Ga}_{1-x}\text{N}$ has an alloy fraction close to $\text{In}_{0.53}\text{Ga}_{0.47}\text{N}$.

2. Model Description

Figure 1 illustrates roughly the $\text{In}_{0.53}\text{Ga}_{0.47}\text{N}/\text{GaAs}$ dual junction structure, where x_j is the junction depth, w is the depletion region width and d is the cell thickness.

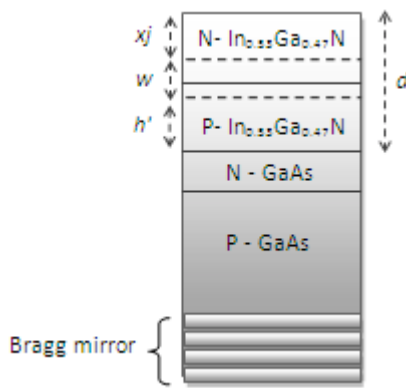


Fig. 1. Simplified configuration of the $\text{In}_{0.53}\text{Ga}_{0.47}\text{N}/\text{GaAs}$ tandem.

In this work, a number of simplifying assumptions were made, including no series resistance losses, no reflection losses and contact shadowing on the front surface. Currents calculation follows the general methodology described in reference [6].

2.1 Analytical Model

The total output current obtained from individual cells under illumination is given as [6]:

$$I_{Total} = I_{Light} - I_{Dark} \quad (1)$$

$$I_{Light} = \int_{\lambda_{min}}^{\lambda_{max}} [I_p(\lambda) + I_n(\lambda) + I_{dr}(\lambda)] d\lambda \quad (2)$$

Where:
 $I_p(\lambda)$ and $I_n(\lambda)$ are respectively photocurrents due to holes and electrons collected at the depletion edges x_j and x_j+w ;

$I_{dr}(\lambda)$ is the photocurrent obtained from the depletion region;
 λ_{min} is the wavelength corresponding for the bottom cell in case of double junction system to the top cell bandgap, and equals zero for the top cell;
 λ_{max} is the wavelength corresponding to the cell bandgap.

The dark current is calculated using the equation:

$$I_{Dark} = I_0 \cdot \left[\exp\left(\frac{qv}{kT}\right) - 1 \right] \quad (3)$$

Where:

q is the electron charge;
 v is the applied voltage;
 k is the Boltzmann constant;
 T is the temperature;
 I_0 is the saturation current calculated using the following expression [6]:

$$I_0 = \frac{qSD_e n_i^2}{L_e N_a} \frac{\frac{S_e L_e}{D_e} \cosh \frac{h'}{L_e} + \sinh \frac{h'}{L_e}}{\frac{S_e L_e}{D_e} \sinh \frac{h'}{L_e} + \cosh \frac{h'}{L_e}} + \frac{qSD_h n_i^2}{L_h N_d} \frac{\frac{S_h L_h}{D_h} \cosh \frac{x_j}{L_h} + \sinh \frac{x_j}{L_h}}{\frac{S_h L_h}{D_h} \sinh \frac{x_j}{L_h} + \cosh \frac{x_j}{L_h}} \quad (4)$$

Where:

n_i is the concentration of intrinsic carrier;
 S is the cell surface;
 $L_{e(h)}$ and $D_{e(h)}$ are respectively the electron (hole) diffusion length and diffusion constant;
 $N_{a(d)}$ is the acceptor (donor) carrier concentration;
 $S_{h(e)}$ is the recombination velocity in the N(P) type region;

The open-circuit voltage formula is [6]:

$$V_{oc} = \frac{kT}{q} \ln\left(\frac{I_{sc}}{I_0} + 1\right) \quad (5)$$

Where I_{sc} is the short-circuit current.

The global V_{oc} is the addition of the contribution of individual cells:

$$V_{oc} = \sum_{i=1}^n v_{oc,i} \quad (6)$$

Where n is the sub-cells number.

The cell output power is given as:

$$P = I_{Total} \cdot V \quad (7)$$

The cell conversion efficiency is generally given as:

$$\eta = \frac{I_m \cdot V_m}{P_{inc}} \quad (8)$$

Where the product I_m by V_m is the maximum power and P_{inc} is the total incident solar power.

The fill factor is calculated using the following formula:

$$FF = \frac{I_m \cdot V_m}{I_{sc} \cdot v_{oc}} \quad (9)$$

2.2 $In_xGa_{1-x}N$ Parameter Equations Used in Our Program

The equation relating the bandgap energy to the mole fraction x is given as [7,8]:

$$Eg(x) = x \cdot Eg(InN) + (1-x) \cdot Eg(GaN) - x \cdot (1-x) \cdot C \quad (10)$$

Where: $Eg(InN) = 0.7eV$, $Eg(GaN) = 3.42eV$ and C is a bowing parameter which is taken to be equal to 1.43.

Doping concentration dependence of mobility is given by [9]:

$$\mu_i(N) = \mu_{min,i} + \frac{\mu_{max,i} - \mu_{min,i}}{1 + \left(\frac{N}{N_{g,i}}\right)^{\gamma_i}} \quad (11)$$

Where i represent either electrons (e) or holes (h), N is the doping concentration and the specific parameters μ_{min} , μ_{max} , γ and N_g are given in **Table 1**.

Table 1. Parameters for mobility calculation.

Material	$\mu_{min,e}$ [cm ² /vs]	$\mu_{max,e}$ [cm ² /vs]	$\mu_{min,h}$ [cm ² /vs]	$\mu_{max,h}$ [cm ² /vs]
GaN	55	1000	3	170
InN	30	1100	3	340
Material	γ_e	γ_h	$N_{g,e}$ [cm ⁻³]	$N_{g,h}$ [cm ⁻³]
GaN	1	2	$2e^{17}$	$3e^{17}$
InN	1	2	$2e^{17}$	$3e^{17}$

$In_xGa_{1-x}N$ electronic mobility is the linear interpolation between the Indium Nitride and Gallium Nitride values; however, holes mobility of the $In_xGa_{1-x}N$ alloys is assumed to be similar to the GaN holes mobility.

The absorption coefficient of the received radiation energy $E(eV)$, by $In_xGa_{1-x}N$ alloys is taken to be [10]:

$$\alpha(E) = 10^5 \times \sqrt{a \cdot (E - Eg) + b \cdot (E - Eg)^2} \quad (12)$$

a and b are dimensionless fitting constants (**Table 2**).

Table 2. Fitting constants for $In_xGa_{1-x}N$ absorption coefficient.

Indium composition	a	b
0.57	0.60946	0.62182
0.69	0.58108	0.66902
0.83	0.66796	0.68886

The relative dielectric constant for InN and GaN are 10.5 and 8.9 respectively [11,12], so a linear interpolation has been made to find the relative dielectric constant of the $In_xGa_{1-x}N$ alloys.

The electron and hole effective masses were determined using the following equations [13]:

$$m_e^* = m_0 \cdot (0.2 - 0.105 \cdot x) \quad (13)$$

$$m_h^* = m_0 \cdot (1.25 - 0.8 \cdot x) \quad (14)$$

Where m_0 is the electron rest mass.

2.3 GaAs Parameter Equations Used in Our Program

The equation relating the bandgap energy to the temperature is given as [14]:

$$E_g(T) = 1.519 - \frac{5.405 \times 10^{-4} \times T^2}{204 + T} \quad (15)$$

The mobility of electrons and holes can be calculated considering the lattice scattering using the formulas [15]:

$$\mu_e = 8500 \times \left(\frac{T}{300}\right)^{-1} \quad (16)$$

$$\mu_h = 400 \times \left(\frac{T}{300}\right)^{-2.1} \quad (17)$$

According to reference [16], we have used the following law to calculate the absorption coefficient:

$$\alpha(E) = 57125 \times E^2 - 76265 \times E - 6400 \quad (18)$$

In this work, we have taken for the calculation of the static dielectric constant the law given in reference [17]:

$$\epsilon_r(GaAs) = 12.8 \times \left(1 + 9 \times 10^{-5} \times T \right) \tag{19}$$

2.4 Bragg Reflector Design

The net reflectivity R_i at layer i is given by [18]:

$$R_i = \frac{\rho_i + R_{i+1} e^{-2j\beta_i l_i \cos(\theta_i)}}{1 + \rho_i R_{i+1} e^{-2j\beta_i l_i \cos(\theta_i)}} \tag{20}$$

Where:

$$\rho_i = \frac{n_i - n_{i-1}}{n_i + n_{i-1}} \tag{21}$$

$$\beta_i = \frac{2\pi n_i}{\lambda} \tag{22}$$

θ_i is the propagation angle in the i^{th} layer;
 ρ_i is the local reflectivity between layers i and $i-1$;
 β_i , $l_i \cos(\theta_i)$ and n_i are respectively the propagation constant, the effective thickness and the refractive index of the i^{th} layer.

The reflectivity spectrum of the BR depends on the refractive index difference of the two materials. The higher the difference, the higher the reflectivity will be at smaller wavelengths. The reflectivity also depends on the number of pairs. If we increase the number of alternating layer pairs, then the net reflectivity will increase. This is due to the fact that there will be more constructive interference throughout the BR structure.

In our structure, the Bragg reflector with the reflectance upper limit centered at the wavelength range 800nm-900nm consists of a fourteen pairs of GaAs/AlAs layers. The light is supposed incident normal to the BR surface. Thickness of the GaAs layer is 61nm and AlAs thickness is 74nm. These BR selectively reflect transmitted photons with energies near the GaAs bandgap.

Figure 2 below shows the reflectivity spectrum of our Bragg reflectors structure, at a target wavelength of 878nm, where the refractive index of the GaAs layer is 3.61 [19], and that of the AlAs layer is 2.97 [20].

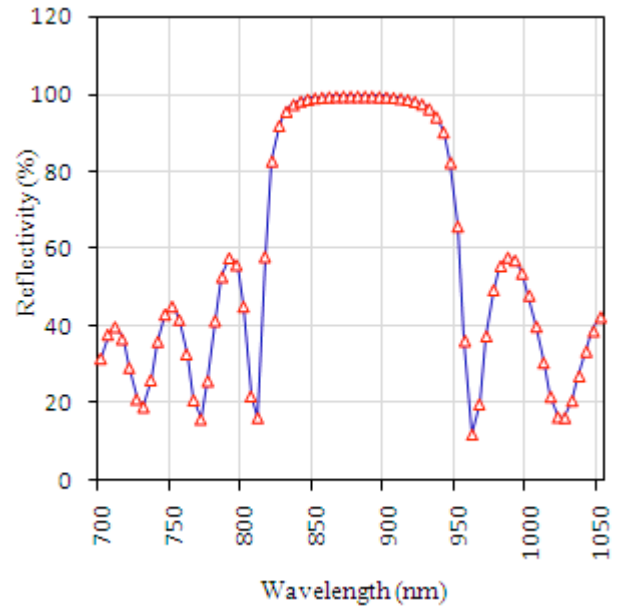


Fig. 2. Reflectance characteristics with 14 BR layers against the wavelength of incident light. The reflectivity of this structure is 98.30%, with a bandwidth of 100nm due to a relatively large refractive index difference of the two materials ($\Delta n = 0.64$).

3. Results and Discussion

The analysis starts by assuming the physical and geometrical parameter values of the two-junctions presented in Table 3.

Table 3. Physical and geometrical parameters used in simulation.

Solar cell	Eg [ev]	Na [cm ⁻³]	Nd [cm ⁻³]	τ_e [s]	τ_h [s]
In _{0.53} Ga _{0.47} N GaAs	1.622 1.422	1e ¹⁷ 1e ¹⁷	5e ¹⁶ 1e ¹⁶	4e ⁻⁹ 1e ⁻⁸	4e ⁻⁹ 1e ⁻⁸
Solar cell	S _e [cm/s]	S _h [cm/s]	x _j [μm]	d [μm]	T [k]
In _{0.53} Ga _{0.47} N GaAs	1e ³ 1e ⁵	1e ³ 1e ⁵	2e ⁻¹ 3e ⁻¹	3 10	300 300

3.1 In_{0.53}Ga_{0.47}N Minority Carrier Lifetimes Effect on η

Figure 3 shows the results of simulation of the consequence that minor lifetimes of the In_{0.53}Ga_{0.47}N sub-cell would have on tandem performance.

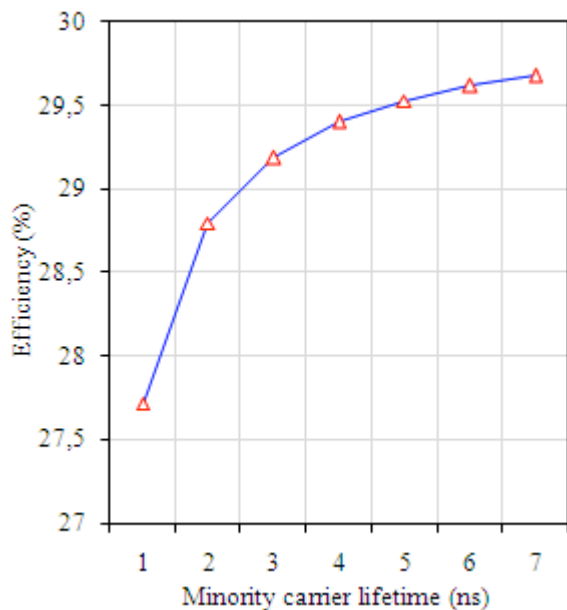


Fig. 3. Effect of minority carrier lifetimes of the $\text{In}_{0.53}\text{Ga}_{0.47}\text{N}$ junction on η .

$\text{In}_x\text{Ga}_{1-x}\text{N}$ alloys have a large absorption coefficient in the direct bandgap, so most of the electron-hole pairs will be created less than a diffusion length away from the junction. As a result, for short carrier lifetimes, the carriers recombine quickly what implies a reduction in the conversion efficiency.

Based on references [21,22], the lifetime of holes in GaN and InN can reach respectively 6.5ns and 5.4ns. However, $\text{In}_x\text{Ga}_{1-x}\text{N}$ alloys are expected to have inferior lifetimes owing to compositional fluctuations. Thus, we assumed in our calculations, for electrons and holes, a 4ns minority carrier lifetime.

3.2 Simulation of the $I(V)$ characteristics

The $I(V)$ characteristics of single junctions and that of the tandem are calculated and presented on Figures 4 and 5.

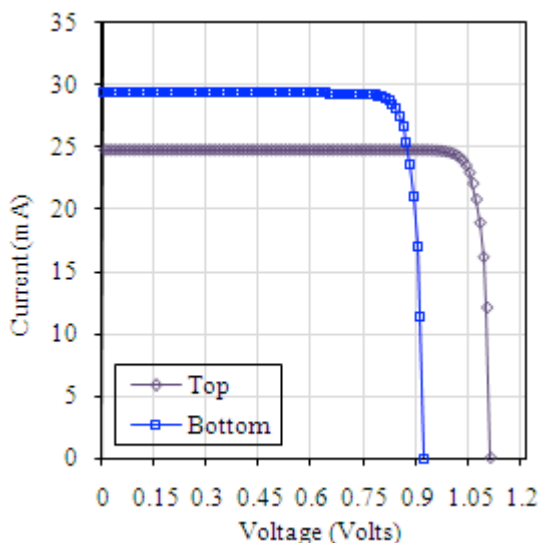


Fig. 4. $I(V)$ characteristics of $\text{In}_{0.53}\text{Ga}_{0.47}\text{N}/\text{GaAs}$ tandem for top and bottom single junctions.

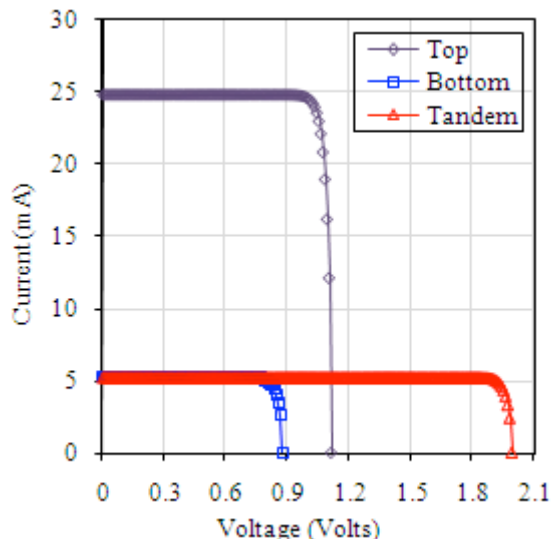


Fig. 5. $I(V)$ characteristics of $\text{In}_{0.53}\text{Ga}_{0.47}\text{N}/\text{GaAs}$ tandem for top, bottom and the tandem.

Table 4. Photovoltaic parameters of the $\text{In}_{0.53}\text{Ga}_{0.47}\text{N}/\text{GaAs}$ tandem.

Solar cell (1-sun AM1.5)	Voc [V]	Isc [mA]	FF [%]	η [%]
Top cell	01.12	24.82	88.50	25.28
Single bottom cell	00.92	29.51	87.09	24.41
Bottom cell	00.87	05.24	86.97	04.12
Tandem	01.99	05.24	93.12	29.40

According to **Table 4** and the preceding curves, one notes that, the current-voltage curve of the $\text{In}_{0.53}\text{Ga}_{0.47}\text{N}$ cell stayed the same, while the current-voltage curve of the GaAs cell had a current drop. This current decrease was expected because the incident spectrum was diminished while crossing the top cell, and since the junctions are mechanically stacked in series, the overall current-voltage characteristic is limited in its current level by the characteristic with the lowest current. In addition, we note a significant increase in efficiency from single junctions to the tandem.

Our calculations predict an efficiency of 29.40%, for the $\text{In}_{0.53}\text{Ga}_{0.47}\text{N}/\text{GaAs}$ tandem by using realistic parameters. This result is similar to that given by GaInP/GaAs based double hetero-junction cells (~30%) [23,24], and better than that obtained for InGaN/Si double-junction tandem solar cells (~27%) [25].

3.3 Effect of $\text{In}_{0.53}\text{Ga}_{0.47}\text{N}$ Front Recombination Velocity on η

Figure 6 illustrates the $I(V)$ characteristics of the tandem as a function of the front recombination velocity (S_h) of the $\text{In}_{0.53}\text{Ga}_{0.47}\text{N}$ sub-cell. While the back surface recombination velocity (S_e) remain fixed at $1\text{e}^3\text{cm/s}$.

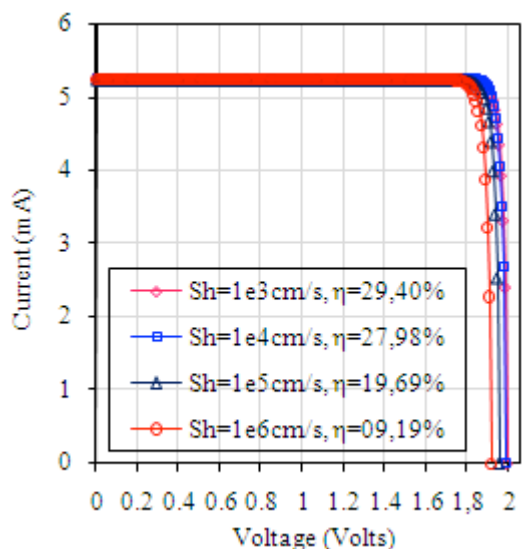


Fig. 6. Simulated $I(V)$ characteristics of the $In_{0.53}Ga_{0.47}N/GaAs$ tandem for various front recombination velocities.

S_h varies widely because it depends on the state of the surface. A $1e^3 - 1e^6$ cm/s S_h variation shows that it affects not simply I_{sc} , but also V_{oc} very considerably for the reason that the increase of recombination process cause an increase of the saturation current (equation 4), at a fixed bias voltage, and consequently V_{oc} (equation 5). Therefore, the conversion efficiency drops remarkably with increasing S_h , in view of the fact that the majority of the carrier generated cannot be gathered, causing a decrease of the electric current. Hence, to diminish the power loss, S_h must not surpass $1e^3$ cm/s.

3.4 Effect of the GaAs Cell Thickness on η

Figure 7 shows a significant variation of the tandem's conversion efficiency when increasing the thickness of the GaAs cell.

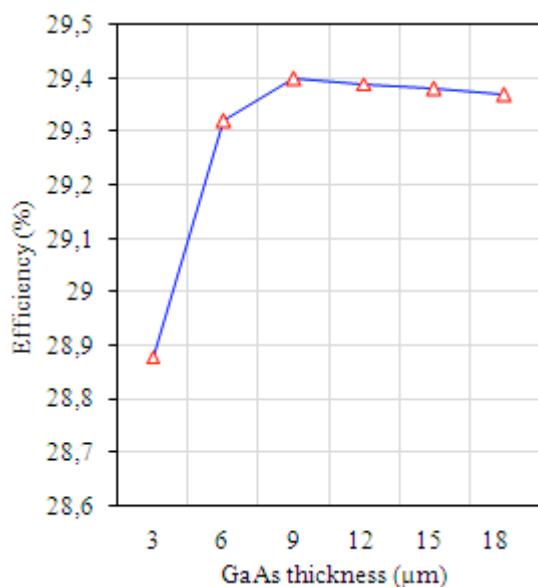


Fig. 7. Influence of the GaAs thickness on η

We note an improvement from 28.88% to 29.40% for $3\mu m$ and $9\mu m$ GaAs cell thickness respectively. Because, the majority of the incident photons, in case of small thickness, are not captivated resulting in a minor efficiency. On the other hand, when the thickness of the cell surpass $10\mu m$, the recombination process causes a slight decrease in the conversion efficiency, because the largest part of the free carriers created away from the electrodes will recombine before reaching the electrodes. Therefore, a GaAs cell width of approximately $10\mu m$ is required.

3.5 Influence of Changing the Operating Temperature on η

Through simulation of the reliance between device temperature and its output photovoltaic parameters, we can predict its performance for realistic use.

$I(V)$ characteristics of the tandem are shown in figure 8, while I_0 , V_{oc} , I_{sc} , η and FF are listed in table 5.

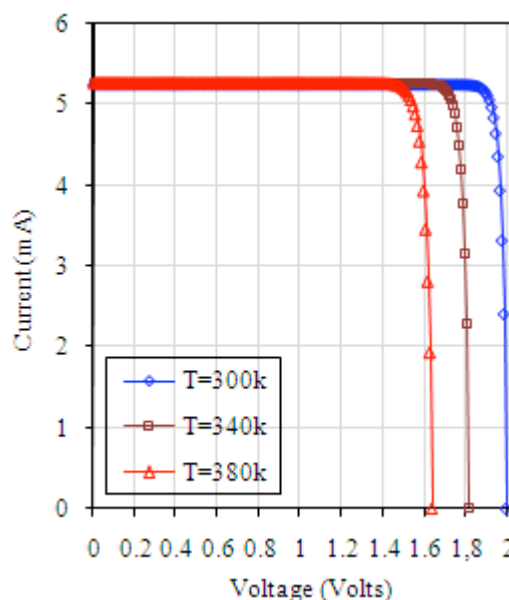


Fig. 8. $I(V)$ characteristics of the tandem for various Temperatures.

The decrease of V_{oc} , observed with increasing temperature, is due to enhance of I_0 . This is the result of reduction in bandgaps, causing also a feeble improve of I_{sc} due to enhancement in carrier's production mechanisms.

Therefore, while the decrease of V_{oc} is more important than the increase of I_{sc} , both the fill factor and the conversion efficiency will decrease with increasing temperature (Figure 9).

Table 5. Influence of T on the photovoltaic parameters.

T (k)	300			340			380			
	Cell	Top	Bottom	Tandem	Top	Bottom	Tandem	Top	Bottom	Tandem
I_0 (A)		$4.30e^{-21}$	$9.57e^{-18}$	-	$1.03e^{-17}$	$1.59e^{-14}$	-	$4.94e^{-15}$	$5.78e^{-12}$	-
V_{oc} (V)		01.12	0.88	01.99	01.04	0.77	01.82	0.96	0.67	01.63
I_{sc} (mA)		24.82	05.24	05.24	24.89	05.27	05.27	24.95	05.29	05.29
FF (%)		88.50	86.97	93.12	87.33	84.31	91.83	85.39	81.21	90.32
η (%)		25.28	04.12	29.40	23.24	03.55	26.80	21.02	02.98	24.01

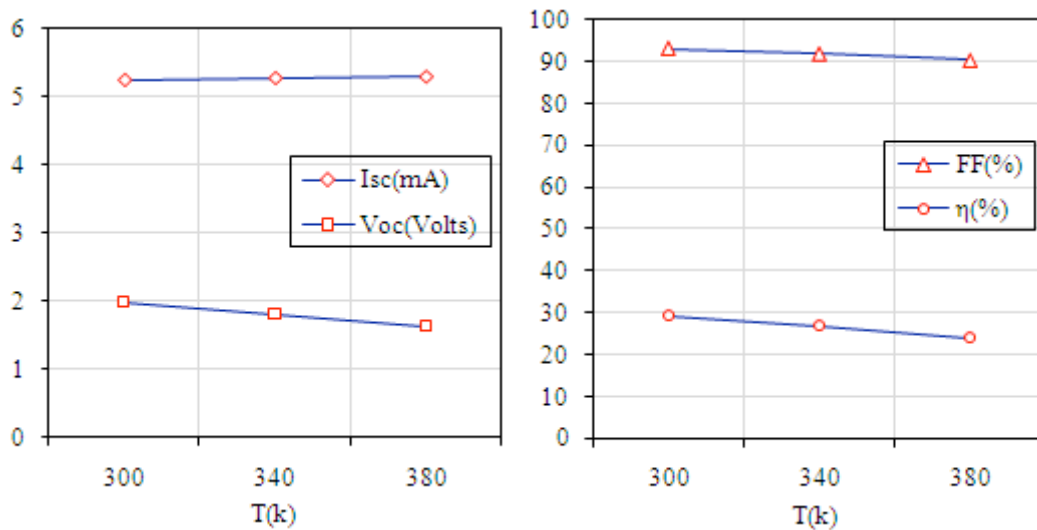


Fig. 9. Influence of T : (Left) on V_{oc} and I_{sc} , (Right) on FF and η of the tandem.

4. Conclusion

In this paper, theoretical efficiency potential of double junction $In_{0.53}Ga_{0.47}N/GaAs$ tandem under 1-sun AM1.5 illumination, including Bragg mirror rear surface reflector, is investigated using realistic parameters by numerical simulation. It is found that higher surface recombination velocities at the top $In_{0.53}Ga_{0.47}N$ cell causes a considerable drop of the conversion efficiency. So, it is imperative to maintain the front recombination velocity less than $1e^3$ cm/s for high conversion efficiency. Furthermore, a cell thickness of about $10\mu m$ is more advantaged because of the recombination phenomenon.

In addition, we have analyzed the temperature sensitivity of our structure and we found that the augment of temperature causes a degradation of the tandem's performance.

References

[1] Q. Rüdiger, *Gallium Nitride Electronics*, Springer-Verlag, Berlin Heidelberg, 2008.
 [2] X. Shen, S. Lin, F. Li, Y. Wie, S. Zhong, H. Wan, J. Li, "Simulation of the InGaN-based tandem solar

cells", *Photovoltaic Cell and Module Technologies II*, Edited by Bolko von Roedern, Alan E. Delahoy, Proceedings of Spie, Vol. 7045-E, 2008.

[3] K. Nandy, S. Biswas, R. Bhattacharyya, S. N. Saha, A. Deyasi, "Novel Band-Reject Filter Design Using Multilayer Bragg Mirror at 1550 nm", *Computer Science & Information Technology*, ACER 2013, pp. 419-425, 2013.
 [4] I. I. Ivanov, T. V. Nychyporuk, V. A. Skryshevsky, M. Lemiti, "Thin silicon solar cells with $SiOx/SiNx$ Bragg mirror rear surface reflector", *Semiconductor Physics, Quantum Electronics, Optoelectronics*, V. 12, N 4, pp. 406-411, 2009.
 [5] R. H. Sara, M. J. A. de Dood, and H. Kim, "Ultrafast optical response of a high-reflectivity GaAs/AlAs Bragg mirror", *Appl. Phys. Lett.*, 86, 031109.1-3, 2005.
 [6] S. M. Sze and K. K. Ng, *Physics of Semiconductor Devices*, Third Edition, John Wiley, Interscience, 2006.

- [7] J. Wu and W. Walukiewicz, "Bandgaps of InN and group III nitride alloys", *Super lattice. Microst.*, 34, pp.63-75, 2003.
- [8] J. Wu, "When group III-nitrides go infrared: new properties and perspectives", *J. of Appl. Phys.*, Vol. 106, 011101-1-28, 2009.
- [9] T. T. Mnatsakanov, M. E. Levinshtein, L. I. Pomortseva, S. N. Yurkov, G. S. Simin, and M. Asif Khan, "Carrier mobility model for GaN", *Solid-State Electron*, 47, pp.111-115, 2003.
- [10] J. F. Muth, J. H. Lee, I. K. Shmagin, R. M. Kolbas, H. C. Caser, B. P. Keller, U. K. Mishra and S. P. Den Baars, "Absorption coefficient, energy gap, exciton binding energy, and recombination lifetime of GaN obtained from transmission measurements", *Appl. Phys. Lett*, 71, pp.2572-2574, 1997.
- [11] M. E. Levinshtein, S. L. Rumyantsev and M. S. Shur, *Properties of Advanced Semiconductor Materials: GaN, AlN, InN, BN, SiC, SiGe*, John Wiley and Sons, Inc. New York, 2001.
- [12] T. Inushima, M. Higashiwaki and T. Matsui, "Optical properties of Si-doped InN grown on sapphire (0001)", *Phys. Rev.*, B68: 235204-1-7, 2003.
- [13] S. N. Mohammad, A. A. Salvador and H. Morkoç, "Emerging Gallium Nitride Based Devices", *Proceedings of the IEEE*, Vol. 83(10), 1995.
- [14] Ioffe Physico-Technical Institute:
<http://www.ioffe.rssi.ru/SVA/NSM/Semicond/GaSb/bandstr.html>
- [15] S. Siegfried, *Analysis and simulation of semiconductor devices*, Springer-Verlag, 1984.
- [16] B. O. Seraphin, "Solar energy conversion: Solid-state physics aspects", *Topics in appl. Phys.*, Vol 31, Springer-Verlag, 1997.
- [17] J. S. Blakemore, "Semiconducting and other major properties of gallium arsenide", *J. of Appl. Phys.*, 52(10), pp.123-181, 1982.
- [18] J. Connie, C. Hasnain, *Vertical Cavity Surface Emitting Lasers, Semiconductor Lasers: Past, Present, and Future*, American Institute of Physics Press, Woodbury, NY, Aug., 1995.
- [19] D. E. Palik, *Handbook of Optical Constants of Solids*, Volumes I, II, and III, Elsevier Science & Tech, 1985.
- [20] M. Bass, C. DeCusatis, J. Enoch, V. Lakshminarayanan, G. Li, C. MacDonald, V. Mahajan, E. Van Stryland, *Handbook of Optics, Optical Properties of Materials, Nonlinear Optics, Quantum Optics*, Third Edition, Vol IV, McGraw-Hill, 2009.
- [21] Z. Z. Bandic, P. M. Bridger, E. C. Piquette, T. C. Mc Gill, "Minority carrier diffusion length and lifetime in GaN", *Appl. Phys. Lett*, 72, pp.3166-3168, 1998.
- [22] F. Chen, A.N. Cartwright, H. Lu, W. J. Schaff, "Temperature dependence of carrier lifetimes in InN", *Appl. Phys. Lett*, 87, 212104-1-3, 2005.
- [23] T. Takamoto, T. Agui, E. Ikeda and H. Kuri, "High efficiency InGaP/InGaAs tandem solar cells lattice-matched to Ge substrates", *Solar Energy Materials and Solar Cells*, 66, pp.511-517, 2001.
- [24] T. Takamoto, E. Ikeda, H. Kurita and M. Ohmori, "Over 30% efficient InGaP/GaAs tandem solar cells", *Appl. Phys. Lett*, 70, pp.381-383, 1997.
- [25] L. Hsu and W. Walukiewicz, "Modelling of InGaN/Si tandem solar cells", *J. of Appl. Phys.*, 104: 024507, 2008.